Enhanced hybrid lidar-radar ranging technique

David W. Illig, William D. Jemison, Luke Rumbaugh
Department of Electrical and Computer Engineering
Clarkson University
Potsdam, NY
illigdw@clarkson.edu

Robert Lee, Alan Laux, Linda Mullen
EO and Special Mission Sensors Division
NAVAIR
Patuxent River, MD

***Abstract*—A new hybrid lidar-radar underwater ranging technique is presented to enhance optical ranging in underwater environments. This technique has the potential to extend the unambiguous range by an order of magnitude while maintaining range precision that is comparable to existing techniques. The technique combines frequency domain reflectometry (FDR) [1] and modulated continuous wave (CW) ranging [2] to simultaneously achieve good unambiguous range and range precision performance. Theory and simulation are presented to demonstrate the FDR and combined FDR/CW approach. These results indicate that for the system parameters chosen the combined FDR/CW approach can extend the unambiguous range from tens of centimeters to approximately ten meters depending on water turbidity while maintaining the range precision associated with the CW approach.**

Keywords—underwater, optical, ranging, scattering

I. Introduction

Underwater detection has traditionally been performed through the use of acoustic approaches which are good for long distance ranging. However, these methods provide relatively low range resolution. Hybrid lidar-radar has also been used to perform underwater detection, ranging, and imaging and offers the ability to provide high resolution and accuracy for short distance ranging [3]. Hybrid lidar-radar is an optical technique in which radar-like intensity modulation is applied to laser light in order to improve system performance.

Optical absorption and scattering provide substantial challenges for hybrid lidar-radar systems. Absorption of photons by the water channel causes the power of the received signal to decrease. The effects of absorption can be reduced by choosing the laser wavelength to be in the blue-green region. Scattering occurs when photons in the collimated laser beam are reflected by particulates in the channel, causing the beam to spread. The optical power transmitted through the channel decays exponentially as a function of the absorption coefficient, a, and the scattering coefficient, b:

$$P(z) = P_0 e^{-(a+b)z} = P_0 e^{-cz} \tag{1}$$

where z is the distance between the object and the hybrid lidar-radar system. The effects of absorption and scattering are often combined into a single parameter, the beam attenuation coefficient, c.

Of particular concern is backscattering, which occurs when a photon is reflected off a particulate and reaches the detector without first reaching the desired object. Backscattered light contains no information regarding the desired object, reducing image contrast, resolution, and range accuracy. Several methods have been developed to mitigate the effects of backscatter. One approach is to select a modulation frequency of at least 100 MHz, as backscatter magnitude has been shown to decrease for high modulation frequencies [4]. Another technique uses a dual high-frequency approach in order to suppress backscatter while also obtaining a larger unambiguous range than a single frequency technique [2]. A third approach applies a simple delay line filter to cancel backscattering in the spatial frequency domain [5]. Techniques based on the use of high modulation frequencies may offer a trade-off in which a high modulation frequency can lead to backscatter reduction, but a lower modulation frequency is often desirable to obtain large unambiguous range.

This paper presents a new ranging technique that borrows from the frequency-domain reflectometry (FDR) technique used in the microwave and fiber optics community to detect faults in very long cables [1]. The FDR technique can substantially increase the unambiguous range of hybrid lidar-radar systems while maintaining a substantial backscatter reduction capability. Section II briefly discusses the hybrid lidar-radar system, some previous ranging techniques, and the theory behind the FDR technique. In Section III, the setup and procedure for the simulations will be presented. Simulated data will be presented in Section IV. Section V discusses the advantages and disadvantages of the new method and provides areas for future work. Finally, Section VI provides conclusions summarizing the results of this work.

II. Background

A block diagram of a simplified hybrid lidar-radar system is shown in Figure 1. The transmitted laser light is modulated by a RF radar signal. The modulated optical signal enters the underwater channel where an object of interest is located. Light reflected from the object as well as backscattered light is collected by an optical detector, where it is converted into an electrical signal. This electrical signal is digitized by a software-defined radio, where it is also demodulated into its in-phase (I) and quadrature (Q) components. The I and Q signals can then be processed to obtain the magnitude and phase of the radar subcarrier relative to the transmitted modulation envelope. Two previous ranging methods will briefly be summarized, followed by an overview of the theory

978-0-933957-40-4 ©2013 MTS

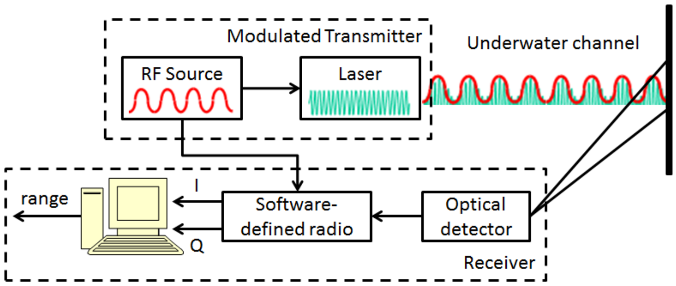

Figure 1. Simplified hybrid lidar-radar block diagram

behind the FDR ranging technique and the motivation for the combined FDR/CW approach.

A. Single modulation frequency CW hybrid lidar-radar

In the single frequency CW approach, a single sinusoidal signal is used as the modulation signal for the laser. The range to an object may be calculated from the change in phase of the return signal relative to a reference position:

$$R = \frac{\Delta\varphi}{4\pi}\lambda \quad (2)$$

where R is the range to the object, $\Delta\varphi$ is the change in phase relative to the reference phase, and λ is the wavelength of the modulating waveform.

The unambiguous range of the single frequency approach is limited by the wavelength of the modulation frequency. Both the unambiguous range d_{UNAMB} and the range precision δd can be expressed in terms of the wavelength or the modulation frequency f_m [2]:

$$d_{UNAMB} = \frac{\lambda}{2} = \frac{v}{2f_m} \quad (3)$$

$$\delta d = \frac{\delta\varphi}{4\pi}\lambda = \frac{v}{4\pi f_m}\delta\varphi \quad (4)$$

where v is the speed of light in the medium and $\delta\varphi$ is the precision of the phase shift measurement.

The single frequency approach presents a tradeoff between unambiguous range and precision, as both quantities depend on the modulation frequency. Additionally, there is a tradeoff between unambiguous range and backscatter reduction. A high modulation frequency is needed to suppress backscatter, but a low modulation frequency is needed to obtain a large unambiguous range.

B. Dual modulation frequency CW hybrid lidar-radar

The dual frequency CW approach was developed to provide increased unambiguous range while also achieving high precision ranging and backscatter suppression. The approach uses a pair of sinusoidal modulation signals f_1 and f_2 that are both greater than 100 MHz. The difference between the frequencies $(f_2 - f_1)$ determines the unambiguous range and range precision [2]:

$$d_{UNAMB} = \frac{v}{2(f_2 - f_1)} \quad (5)$$

$$\delta d = \frac{v}{4\pi(f_2 - f_1)}(\delta\varphi_2 - \delta\varphi_1) \quad (6)$$

Although the backscatter is reduced due to the use of high modulation frequencies, the range precision is reduced as it now depends on the frequency difference rather than the individual modulation frequencies. Additionally, there is a tradeoff between unambiguous range and precision as both depend on the frequency difference. However, the range precision can be improved by using the phase shift of one of the dual frequencies to obtain higher precision as in the single frequency CW method using (4).

C. Frequency-domain reflectometry

The frequency-domain reflectometry technique was originally developed in the 1980s to characterize fiber optic lasers [6,7]. The technique has since been used in a wide variety of applications where a large unambiguous range and high precision are desirable traits, such as structural health monitoring, detection of faults in aircraft wiring, and detection of underground water [8,9,10]. The success of the FDR technique in these applications motivates its adaptation for hybrid lidar-radar systems in order to provide a ranging technique that offered large unambiguous range and good range precision. In some sense the FDR technique is an extension of the dual modulation frequency CW technique, in that it provides extended unambiguous range compared to the single modulation frequency CW technique. As will be shown, the FDR method provides significantly more information than the dual modulation frequency CW method, in the form of an instantaneous channel response.

In the FDR method, measurements are made in the frequency-domain and transformed into the time-domain to obtain range information. A stepped frequency modulation is applied to the laser transmitter. The receiver records the magnitude and phase of the return signal at each frequency step, yielding a sampled version of the frequency response of the channel. Range information is obtained by applying the inverse Fast Fourier Transform (IFFT) to transform the frequency-domain measurements into time-domain data. Peaks occurring in the time-domain indicate the positions of objects in the channel. As this process obtains data for multiple range bins, the FDR method can be used to simultaneously detect multiple objects in the channel as well as the peak of the volumetric backscatter.

The range equations for the FDR method can be derived from Nyquist theory applied to frequency-domain sampling as shown in Figure 2. The left half of the figure shows a sketch of a sampled frequency-domain signal, while the right half shows a sketch of the corresponding time-domain signal. As with time-domain sampling, the frequency-domain sample spacing Δf defines the maximum sampling "rate" in the time-domain, t_{max}, which is converted to unambiguous range by multiplying by the speed of light:

$$t_{max} = \frac{1}{\Delta f} \quad (7)$$

$$d_{UNAMB} = \frac{v}{2\Delta f} \quad (8)$$

Objects at physical distances greater than the unambiguous range will be aliased as is typical in sampling theory, such that the calculated distance falls within the unambiguous range. The range precision depends on the bandwidth B of the stepped frequency sweep and the number of data points used in the IFFT step. Assuming that all observations are placed in the correct range bins, the minimum resolution for discriminating between two closely spaced objects is equal to half of the bin size. All values falling into a range bin will be mapped to the midpoint of that bin, so two closely spaced objects must be separated by at least half of a range bin to be correctly detected as separate objects. The bin size b can be calculated by partitioning the unambiguous range by the number of tones N in the stepped frequency modulation:

$$b = \frac{1}{2N} d_{UNAMB} = \frac{\nu}{4N\Delta f} = \frac{\nu}{4B} \tag{9}$$

where the product of the number of tones N and the frequency step size Δf yields the modulation bandwidth B because all of the tones are equally spaced in the frequency-domain. Multiple physical range locations may be mapped into the same range bin location, causing the possible range values calculated by the FDR method to be a finite set of "quantized" range locations. This is in contrast to the continuous set of range positions that would be calculated with the single or dual frequency CW approaches. The range precision can be improved by using more points in the IFFT step by zero-padding the signal, which increases the number of range bins [11]. For an IFFT with n points, the range precision is given by:

$$\delta d = \frac{N}{n} * b = \frac{\nu N}{4Bn} \tag{10}$$

Unlike the single frequency CW approach, the FDR technique does not have a tradeoff between unambiguous range and precision, as these depend on the separate quantities of frequency step size and modulation bandwidth, respectively. FDR enhances coherent reflections from discrete objects compared to reflections from incoherent sources (i.e. distributed backscatter) [6], so FDR should reduce backscattering effects in the underwater channel when sufficiently high modulation frequencies are used.

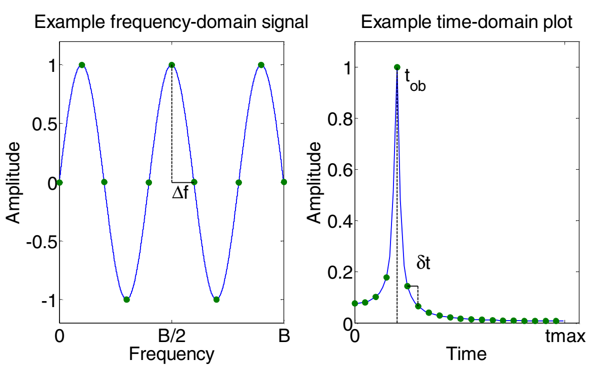

Figure 2. Frequency-domain sampling sketch

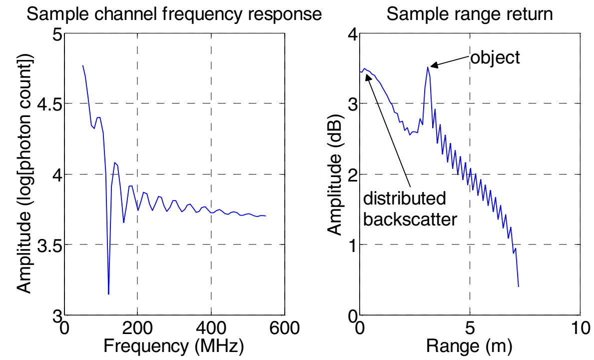

Figure 3. Sample FDR frequency response and range return

A simulated FDR return is shown in Figure 3 for an object placed 3 m away from the system and a turbidity of 2 m^{-1}. This is a harbor-like condition in which the system performance is becoming scatter-limited. The left side of Figure 3 shows the frequency-domain measurements made by the FDR approach, which provides a sampled channel frequency response. It is difficult to discern the object position in the frequency-domain. However, by calculating the IFFT of this frequency response, the time-domain information on the right side of Figure 3 is obtained. A sharp peak is clearly seen at the object position of 3 m, with a broader peak reaching a maximum at 0.22 m representing the volumetric backscatter. The difference in the shapes of the peaks corresponding to a discrete object versus the distributed backscatter can be used to automatically detect the object in the scene. Figure 3 illustrates a key advantage of FDR over the dual frequency CW approach: FDR simultaneously provides range information for all objects illuminated by the laser beam.

D. Combined FDR/CW approach

The single and dual frequency CW approaches are capable of achieving high precision measurements on the order of centimeters, but have relatively low unambiguous ranges due to the dependency of the unambiguous range on the modulation wavelength. The FDR method is able to achieve a large unambiguous range, but requires a bandwidth of several gigahertz to achieve centimeter-order precision, as seen in (10). Currently, such a large bandwidth presents serious technology challenges. This motivates the development of a combined ranging approach, in which an FDR configuration with relatively low bandwidth is used to eliminate range ambiguity while a single frequency CW approach is used to perform high precision ranging measurements. The operation of this combined FDR/CW approach will briefly be described. This procedure uses the ranging measurement obtained by FDR to remove the phase ambiguity inherent in the single frequency CW approach. An illustrative example is sketched in Figure 4 for an object placed 7.9 m away from the system.

First, the FDR approach is used to obtain a coarse range measurement, with the unambiguous range and precision defined by (8) and (10), respectively. The precision of this measurement is limited by the size of the range bin. In the example sketched in Figure 4, the correct range bin has been determined using FDR. However, if the calculated result is the midpoint of the bin, this results in a calculated range of 7.5 m and an error of 0.4 m. Next, a single frequency CW approach is used to measure the range to the object; the frequency should be at least 100 MHz to ensure it is above the backscatter cutoff point [4]. This single frequency provides a high precision measurement; however, this measurement is ambiguous according to (3), as sketched in Figure 4. Large range errors are possible in the absence of any additional *a priori* knowledge to eliminate the range ambiguity. In the example of Figure 4, the range is calculated to be 0.4 m, resulting in an error of 7.5 m. A fine range measurement can be made by using the FDR range bin to select the "correct" single frequency range measurement from the set of ambiguous measurements. In this way, the combined FDR/CW ranging approach is able to achieve the large unambiguous range of the FDR approach from (8) while also achieving the high range precision of the single frequency approach CW according to (4). This combined approach would correctly calculate the object position of 7.9 m in the example of Figure 4. Under the combined approach, FDR can be used periodically to ensure that the CW range calculation is still reporting the correct object location, or FDR could be used on every measurement to provide the full channel response. The combined FDR/CW approach will be used in the majority of the simulations presented in the remainder of the paper.

III. SETUP AND PROCEDURE

The parameters listed in Table 1 were used as inputs to the RangeFinder simulation tool, which is used to predict the performance of hybrid lidar-radar systems. This tool is based on the method of moments and solution of the radiative transfer equation in the small-angle diffusion approximation [12]. The stepped frequency modulation waveform used in this work had 64 tones between 50 MHz and 550 MHz, for a modulation bandwidth of 500 MHz and a step size of approximately 7.8 MHz. The number of range bins is set to 128 by using a 128-point IFFT. These parameters correspond to an unambiguous range of 14.4 m and a range precision of 5.63 cm using (8) and (10), respectively. The integration time for each tone was 100 μs. The 550 MHz tone was used as the single frequency CW component to improve range precision. The values in Table 1 were selected for compatibility with the experimental setup that will be used in the future. To ensure that the simulated data will be relevant to future experimental data, the phase function of Maalox® antacid was used as an input to the program [13].

The modulation depth of the blue (450 nm) laser diode proposed for the future experimental work was measured to quantify the extent to which light remains modulated at each frequency, defined as:

$$m(f) = \frac{\frac{1}{2}(P_{max}-P_{min})}{\frac{1}{2}(P_{max}+P_{min})} = \frac{P_{max}-P_{min}}{2P_{ave}} \tag{11}$$

where P_{max} and P_{min} are the maximum and minimum, respectively, of the incoming modulated component of the optical signal and P_{ave} is the non-modulated component. The modulation depth measured over the selected frequency range is shown in Figure 5. Modulation depth is relatively constant up to about 350 MHz, decreasing by only about 10% from its

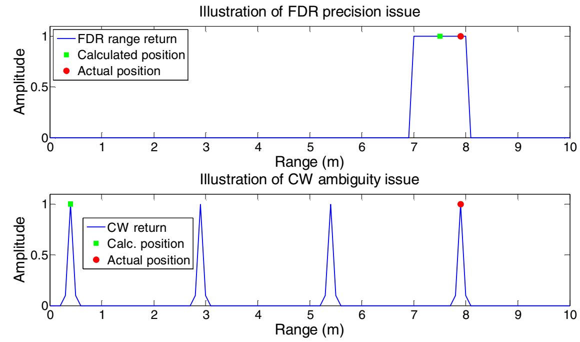

Figure 4. Motivation for combined FDR/CW approach

Table 1. Simulation parameters

Parameter	Value	Unit
System geometry		
Source-receiver separation	0.127	m
Receiver-object distance	1.5 – 3.5	m
Source parameters		
Wavelength	450	nm
Power	50	mW
Aperture size	0.01	m
Field of view	0.2	deg
Modulation frequency	50 – 550	MHz
Receiver parameters		
Aperture	0.0508	m
Field of view	4.7	deg
Optical system transmission	0.5	
Quantum efficiency	0.11	
Analog-to-digital converter bits	14	bits
Object characteristics		
Size (width)	0.3	m
Reflectivity	0.6	
Water characteristics		
Beam attenuation coefficient	0.05 – 2	m^{-1}
Single-scattering albedo	0.9	
Phase function	Maalox® [a]	
FDR/CW configuration		
Bandwidth	500	MHz
Number of tones	64	
Step size	7.8	MHz
Fourier transform bins	128	
Single frequency tone	550	MHz
Integration time	100	μs

a. Reference [13]

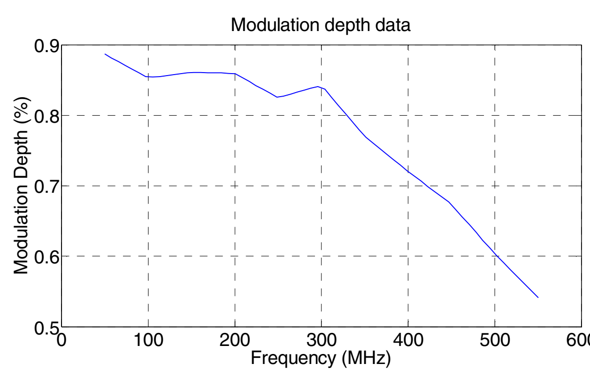

Figure 5. Modulation depth data

maximum value. The rapid loss of modulation beyond this point is believed to result from the modulation frequency approaching the corner frequency of the laser diode driver electronics. The experimentally measured modulation depth values were also used as an input to the simulation.

A. Simulation Details

The photocurrent measured by a hybrid lidar-radar receiver can be expressed as

$$i(r,t) = i_{ob}(r,t) + i_{BSN}(r,t) + i_{noise}(r,t) \tag{12}$$

where r is the distance between the system and the object at time t, $i_{ob}(r,t)$ is the contribution due to the object return, $i_{BSN}(r,t)$ is the contribution due to the backscatter signal, and $i_{noise}(r,t)$ is the contribution due to noise from the photodetection process. The object and backscatter signals can be expressed as:

$$i_{ob}(r,t) = i_{ob}(r)\cos\big(\omega t - \varphi_{ob}(r)\big) \tag{13}$$

$$i_{BSN}(r,t) = i_{BSN}(r)\cos\big(\omega t - \varphi_{BSN}(r)\big) \tag{14}$$

where $i_{ob}(r)$ is the amplitude of the object return, $\varphi_{ob}(r)$ is the phase of the object-reflected modulation envelope, $i_{BSN}(r)$ is the amplitude of the backscatter return, $\varphi_{BSN}(r)$ is the cumulative phase of the backscattered modulated light, and ω is the modulation frequency. Under FDR, the modulation frequency varies throughout the sweep, while it is a constant for the CW ranging technique. The noise term in (12) considers both shot noise and digitization noise. Shot noise is modeled by a Poisson distribution parameterized on the average number of photons arriving at the detector during the integration time [14]. Digitization noise occurs due to the discretization of the receiver's analog to digital converter (ADC), which is modeled by a uniform distribution parameterized by the number of ADC bits and the number of detected photons.

In order to obtain statistics for the performance of the FDR/CW algorithm, a custom Monte Carlo simulation was performed at various integration times. The complex return signal was computed as the average contribution of each of the components in (12) over the specified integration time. RangeFinder directly provides this information for the object and backscatter signals. For the noise term, magnitude and phase information was calculated from the in-phase (I) and quadrature (Q) channels simulated by RangeFinder for the return signal, which incorporate the object and backscatter returns. The I and Q signals are calculated by mixing the return signal with a local oscillator (LO) signal and a copy of the LO signal whose phase is shifted by 90°:

$$I(r,t) = i_{ob}(r)\cos\big(\varphi_{ob}(r)\big) + i_{BSN}(r)\cos\big(\varphi_{BSN}(r)\big) + i_{noise,I}(r,t) \tag{15}$$

$$Q(r,t) = i_{ob}(r)\sin\big(\varphi_{ob}(r)\big) + i_{BSN}(r)\sin\big(\varphi_{BSN}(r)\big) + i_{noise,Q}(r,t) \tag{16}$$

where the local oscillator has demodulated the object and backscatter signals. When a sufficiently large amount of photons are detected, the standard deviation of the noise current i_{noise} after demodulation can be approximated as:

$$\sigma_{noise} = \sqrt{\frac{1}{2}ei_0(r)B_r + \left(\frac{\gamma}{\sqrt{12*2^q}} * 2i_0(r)\right)^2} \tag{17}$$

where e is the charge of an electron, $i_0(r)$ is the photocurrent averaged over the integration time t_r, $B_r = \frac{1}{2t_r}$ is the Nyquist bandwidth corresponding to t_r, and q is the number of ADC bits. The scaling factor γ takes into account that the dynamic range for the ADC may not be perfectly tuned to the maximum value of the photocurrent signal i_0; ideally γ should have a value of one. The linear term under the radical in (17) corresponds to the shot noise variance, while the squared term corresponds to the digitization noise variance. Digitization noise was neglected in the simulations because the simulated ADC has 14 bits, causing the digitization noise to be negligible compared to the shot noise. With the noise contributions calculated, the magnitude, M, and phase, φ, of the noisy return signal can be calculated:

$$M(r,t) = \sqrt{I(r,t)^2 + Q(r,t)^2} \tag{18}$$

$$\varphi(r,t) = \mathrm{atan}\left(\frac{Q(r,t)}{I(r,t)}\right) \tag{19}$$

The magnitude and phase values are used to construct the frequency-domain signal necessary for the FDR processing steps, while the phase value is used to calculate the range under the single modulation frequency CW approach. The system performance is expected to vary as a function of the integration time, t_r, specified in RangeFinder. As the shot noise component is caused by a zero-mean random process, the phase contribution due to noise is expected to approach zero as the integration time is increased. The backscatter contribution is expected to converge to a constant phase as the integration time increases, with this phase representing the location of the volumetric backscatter peak.

IV. Results

This section will present results from RangeFinder simulations for a variety of water conditions and integration times using the parameters listed in Table 1. As turbidity increases, system performance is expected to decrease due to the increased number of scattering and absorption events. Signal-to-noise ratio is expected to increase as integration time increases due to noise contributions being reduced by averaging. This in turn implies that range accuracy should increase as integration time increases.

A. Comparison between FDR and FDR/CW

To further demonstrate the reasoning for the combined FDR/CW approach, a set of simulations were performed with both FDR alone and the combined FDR/CW method. These simulations were performed at a very low turbidity of c=0.05 m^{-1} and ignoring the effects of noise, such that the two processing schemes could be compared directly. The range calculated with each method is plotted in Figure 6. Note that the FDR range calculations show a quantization-like pattern due to object positions being mapped to the center of the closest range bin. By using additional information from a single frequency, the FDR/CW range calculations are a smooth line that has almost completely eliminated the quantization effect of the FDR method. It is also helpful to view the range errors, which are plotted in Figure 7. The error for FDR alone is observed to oscillate between values close to zero and values around half the size of a range bin. On the other hand, the FDR/CW error is observed to be a slowly increasing function that is significantly smaller than the error observed with FDR alone. The slight increase in error as the object range increases is believed to be caused by forward scattering. The maximum error when using FDR/CW is 0.29 cm, while the maximum error when using FDR alone is 6.29 cm. The combined FDR/CW approach has reduced the maximum error by 95% in this very low turbidity scenario, showing the motivation behind using the combined FDR/CW approach over FDR alone.

B. *FDR/CW performance as a function of turbidity*

Several simulations were run to test the performance of FDR/CW as a function of turbidity to assess the effects of water conditions on algorithm performance. The FDR/CW configuration of Table 1 has an unambiguous range of 14.4 m, while the 550 MHz single tone used in this configuration would have an unambiguous range of 20.45 cm if it was used alone. For each turbidity level, three plots are presented. The first plot shows the time-domain channel response measured by the FDR method, indicating the location of the object as well as the peak of the volumetric backscatter. The second plot illustrates the range statistics for each object position, while the third plot shows the range error statistics. All range statistics in this section are based on the model described in the Simulation Details section. Figure 8 shows the channel response obtained in a clean water case where the object is at the maximum distance of 3.6 m. The object peak appears as a sinc function instead of a delta function due to the fact that the IFFT is being performed over a finite set of frequencies. The calculated range for this scenario is shown in Figure 9, with range error plotted

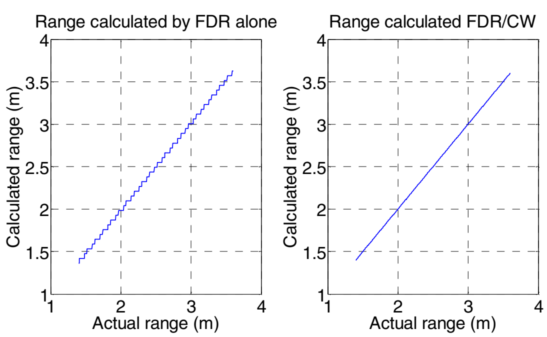

Figure 6. Calculated range comparison between FDR alone and FDR/CW

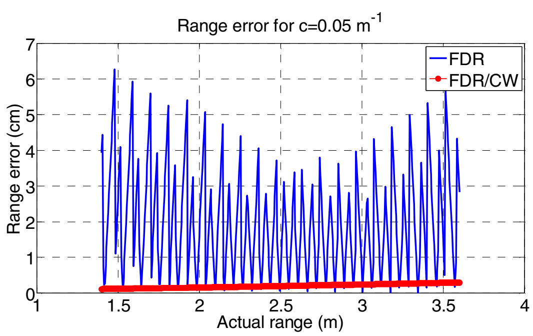

Figure 7. Error comparison of FDR alone to FDR/CW

in Figure 10. The range error is less than one centimeter across the object positions due to the high precision of the CW measurements.

As the turbidity is increased, the peak of the volumetric backscatter increases in amplitude due to the increased scattering, while the object peak decreases due to fewer photons successfully carrying object information to the detector. An example is shown in Figure 11 for the case where $c = 1.25\ m^{-1}$ for an object 3.6 m away from the system. In this scenario, the amplitude of the object peak is approximately 5 dB higher than the amplitude of the peak of the volumetric backscatter. The range for this turbidity is shown in Figure 12, with the range error plotted in Figure 13. Figure 14 shows the channel response for the harbor-like condition of $c = 2\ m^{-1}$ for an object 3.6 m away from the system. Although the object peak is approximately 6 dB lower than the peak of the volumetric backscatter, the object can still be detected due to the different shapes of the two peaks. Figure 15 and Figure 16 show the calculated range and range error for this scenario, respectively. Due to the object and backscatter having similar amplitudes, an interference pattern is observed to occur for objects more than 2.5 m away from the system [2]. This interference pattern also causes small errors to accumulate in the unwrapping process, leading to the offset observed in Figure 16 for the shorter object distances.

These simulation results indicate that for this FDR/CW configuration, the algorithm is able to suppress the effects of scattering until the turbidity reaches $2\ m^{-1}$, at which point performance begins to degrade as evidenced by constructive and destructive interference between the backscatter and object return signals. The channel response plots suggest that the algorithm is able to provide meaningful results for object to backscatter ratios at least as low as -6 dB.

C. *FDR/CW performance as a function of integration time*

In addition to assessing performance at various turbidities, it is important to understand how the FDR/CW method performs for different integration times. As the effects of noise are expected to be more substantial for shorter integration times, there is most likely a tradeoff in a given application between the desired update rate and the system tolerance to noise. This section shows the effects of different dwell times on the CW ranging algorithm.

Performance was assessed for integration times of 1, 10, and 100 μs. The mean range error plus or minus one standard deviation is shown for each integration time for the turbidity conditions of $c=0.05\ m^{-1}$, $c=1.25\ m^{-1}$, and $c=2\ m^{-1}$ in Figure 17, Figure 18, and Figure 19, respectively. The standard deviations are observed to increase as the object distance and turbidity are increased. As expected, increasing the integration time reduces the range error caused by photodetector noise, indicating that integration time may be an important concern when choosing a configuration for FDR/CW. However, changing the integration time does not suppress the range error caused by the interference between the object and backscatter returns seen at the highest turbidity.

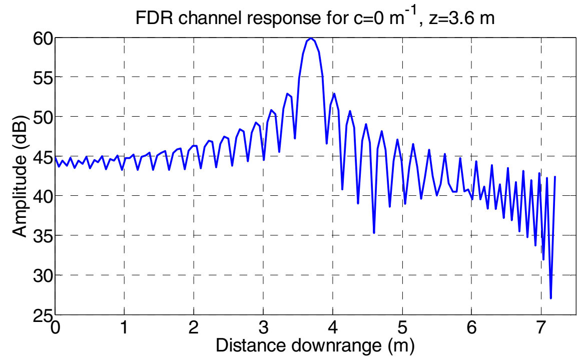

Figure 8. Channel response with object at 3.6 m and c=0 m^{-1}

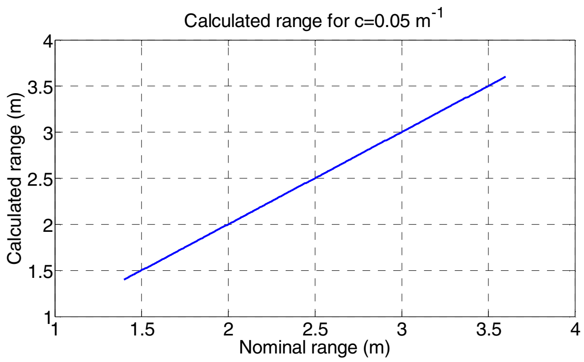

Figure 9. Calculated range with c=0.05 m^{-1}

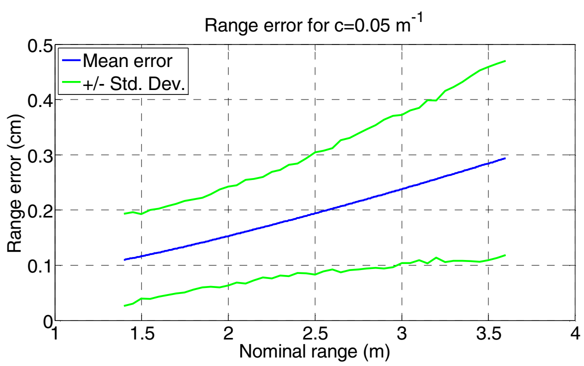

Figure 10. Range error with c=0.05 m^{-1}

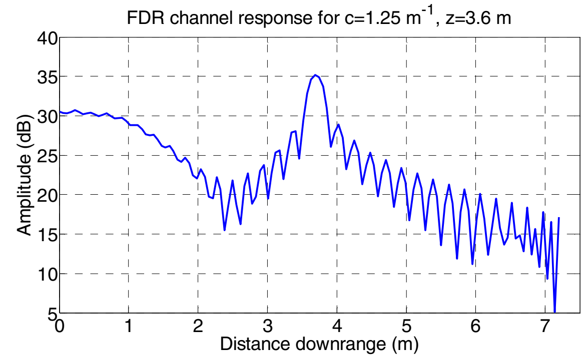

Figure 11. Channel response with object at 3.6 m and c=1.25 m^{-1}

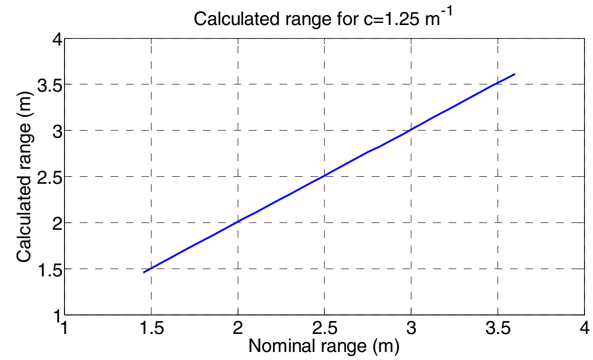

Figure 12. Calculated range with c=1.25 m^{-1}

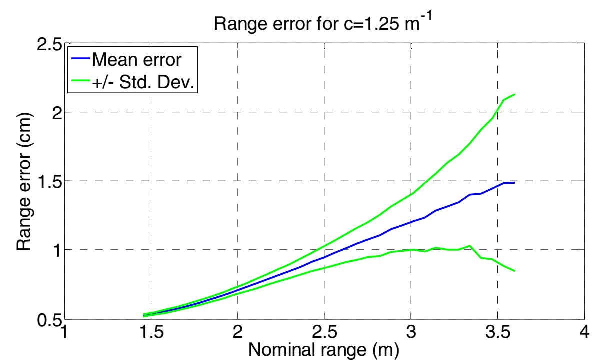

Figure 13. Range error with c=1.25 m^{-1}

V. Discussion and Future Work

This section will briefly compare the new FDR/CW technique to previous methods to illustrate some of the strengths and weaknesses of the new method. This will be followed by a brief discussion of plans for future work with this technique.

The FDR/CW approach offers three main advantages over the previous single and dual frequency CW methods. Perhaps the most substantial advantage is the ability of the FDR/CW approach to calculate the channel response as seen by a hybrid lidar-radar system. This allows FDR/CW to simultaneously detect the location of any objects illuminated by the laser beam as well as the peak of the volumetric backscatter. A second advantage is the ability of the FDR/CW method to achieve large unambiguous range without negatively affecting the range precision. The unambiguous range can be independently designed to meet application requirements by choosing the frequency step size in (8). This is in contrast to the single frequency CW method, where increasing the unambiguous range results in reduced precision. A third advantage is the ability to reduce backscatter without trading off the ability to achieve large unambiguous range. In the single frequency CW approach, a tradeoff exists in which a low modulation frequency is required for large unambiguous range but a high modulation frequency is required for backscatter suppression.

There are also three main disadvantages of the FDR/CW method compared to the single and dual frequency CW approaches. First, the FDR/CW approach requires substantially more processing than these other methods, primarily because FDR/CW requires a Fourier Transform to be calculated. A second issue is the wide bandwidth required by FDR/CW in order to achieve high precision ranging. This has been partially

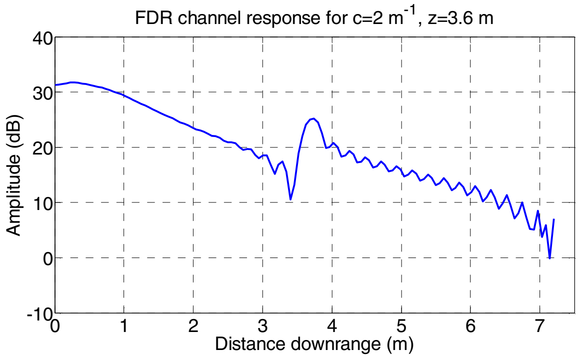

Figure 14. Channel response with object at 3.6 m and c=2 m^{-1}

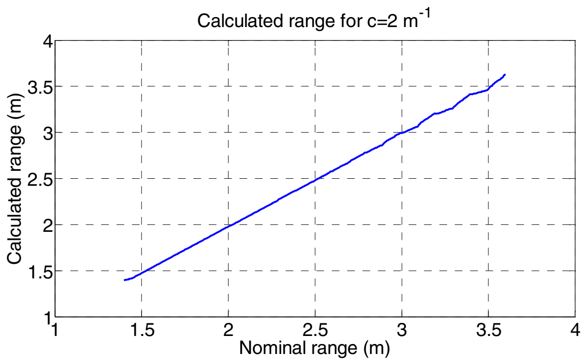

Figure 15. Calculated range with c=2 m^{-1}

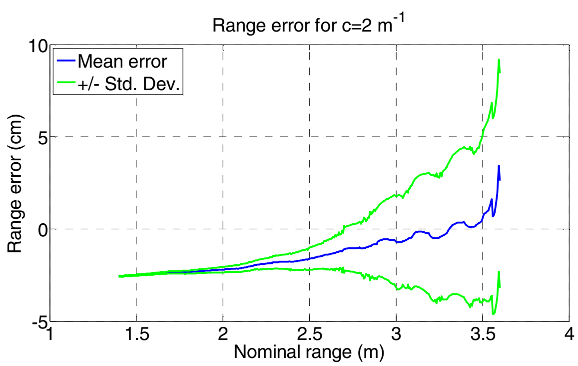

Figure 16. Range error with c=2 m^{-1}

mitigated by using a single frequency CW approach in parallel to the FDR approach, such that the combined method comes close to achieving the precision of the single frequency CW approach. The need to dwell on each of the tones in the FDR/CW approach creates a third challenge. In a practical application, this means that FDR/CW will require a longer amount of time to collect enough data to calculate a range location than a single or dual frequency CW approach which require only one or two measurements, respectively.

A. Future Work

A major area of future work will be to perform experiments further validating the new FDR/CW technique. An experiment has been designed which will utilize the parameters listed in Table 1 to perform investigations similar to those simulated in RangeFinder in a water tank facility at Patuxent River Naval Air Station. The results of this experiment will be compared to

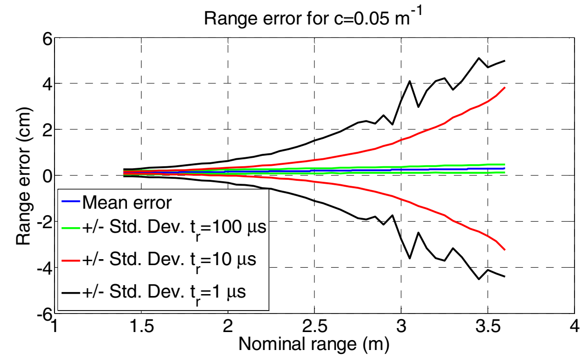

Figure 17. Effect of integration time on error at c=0.05 m^{-1}

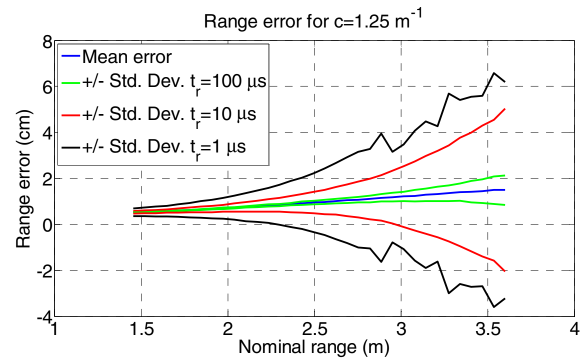

Figure 18. Effect of integration time on error at c=1.25 m^{-1}

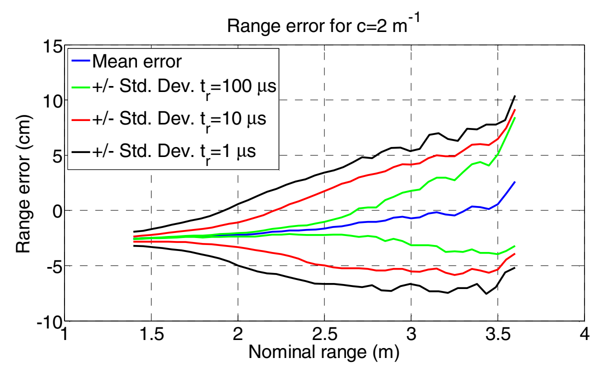

Figure 19. Effect of integration time on error at c=2 m^{-1}

previous experimental work to compare the performance of FDR/CW to other ranging techniques. It may also be beneficial to explore additional FDR/CW parameter configurations to determine the relationships between the number of tones and the bandwidth performance metrics such as range precision and the ability to suppress backscatter.

In terms of algorithm improvement, future work will mainly focus on two tasks. The first of these is to modify the algorithm such that it could be used to detect multiple objects simultaneously. Currently the automated detection algorithm is limited to detecting the strongest object in each return, while an observer manually working with a FDR range spectrum could potentially pick out several objects. The second task is to explore potential algorithms for further backscatter reduction following the FDR/CW processing. This could include adapting spatial filters [5] for the FDR method, or exploring additional sophisticated digital signal processing approaches from radar, communications, or other related fields.

VI. Conclusions

A new hybrid-lidar ranging technique, FDR/CW, has been developed in which large unambiguous range can be achieved without trading off range precision or backscatter reduction capabilities and a channel response can be calculated to indicate the positions of objects of interest and the peak of the volumetric backscatter. The FDR/CW method is able to overcome a major shortcoming of FDR, which is that a bandwidth of several gigahertz is required to achieve centimeter order precision. By using the high precision information of a single frequency CW approach, the FDR/CW method is able to achieve the unambiguous range of FDR and the precision of CW techniques. A specific configuration of FDR/CW was observed to provide accurate ranging results out to at least 3.5 m for turbidities up to a harbor-like condition of $c = 2\ m^{-1}$. The effects of integration time were also explored with a view towards potential practical limitations of this method. Future work will provide further improvements to the algorithm while also collecting a database of experimental data to validate this new approach and compare it to existing approaches.

Acknowledgment

This work is supported by the Office of Naval Research's University Laboratory Initiative (ULI) program contract number N00014-11-1-0371. Any opinions, findings and conclusions or recommendations expressed in this material are those of the authors and do not necessarily reflect the views of the Office of Naval Research.

References

[1] C. Furse, Y.C. Chung, C. Lo, and P. Pendayala. "A critical comparison of reflectometry methods for location of wiring faults," *Smart Structures and Systems*, vol. 2, no. 1, pp. 25-46 (2006).

[2] A. Laux, L. Mullen, P. Perez, and E. Zege. "Underwater laser range finder," *Proc. SPIE 8372, Ocean Sensing and Monitoring IV*, 83721B (2012).

[3] L. Mullen, A.J.C. Vieira, P.R. Herczfeld, and V.M. Contarino. "Application of RADAR technology to aerial LIDAR systems for enhancement of shallow underwater target detection," *IEEE Trans. Microw. Theory Techn.*, vol. 43, no. 9 (1995).

[4] F. Pellen, X. Intes, P. Olivard, Y. Guern, J. Cariou, and J. Lotrian. "Determination of sea-water cut-off frquency by backscattering transfer function measurement," *J. Phys. D: Appl. Phys.*, vol. 33, pp. 349-354 (2000).

[5] P. Perez, W.D. Jemison, L. Mullen, and A. Laux. "Techniques to enhance the performance of hybrid lidar-radar ranging systems," *Proceedings of the IEEE OCEANS 2012 Conference*, Virginia Beach, USA (2012).

[6] R.I. MacDonald. "Frequency domain optical reflectometer," *Applied Optics*, vol. 20, no. 10, pp. 1840-1844 (1981).

[7] W. Eickhoff and R. Ulrich. "Optical frequency domain reflectometry in single-mode fiber," *Applied Physics Letters*, vol. 39, no. 9, pp. 693-695 (1981).

[8] H. Igawa, H. Murayama, T. Kasai, I. Yamaguchi, K. Kageyama, and K. Ohta. "Measurements of strain distributions with a long gauge FBG sensor using optical frequency domain reflectometry," *Proc. SPIE 5855, 17th International Conference on Optical Fibre Sensors*, 547 (2005).

[9] C. Furse, Y.C. Chung, R. Dangol, M. Nielsen, G. Mabey, and R. Woodward. "Frequency-domain reflectometry for on-board testing of aging aircraft wiring," *IEEE Trans. Elecromagn. Compat.*, vol. 45, no. 2, pp. 306-315 (2003).

[10] M.R. Mahmoudzadeh, A.P. Francés, M. Lubczynski, and S. Lambot. "Using ground penetrating radar to investigate the water table depth in weathered granites," *Journal of Applied Geophysics*, vol. 79, pp. 17-26 (2012).

[11] R.J. Schilling and S.L. Harris. *Fundamentals of Digital Signal Processing Using MATLAB*. 2nd ed. Stamford: Cengage Learning (2012).

[12] I.L. Katsev, E.P. Zege, A.S. Prikhach, B.A. Kargin, and A.B. Kargin. "Pulse stretching of the propagated laser beam," *International Workshop on Multiple Scattering Lidar Experiments (MUSCLE-13)*, St. Petersburg, Russia (2004).

[13] A. Laux, R. Billmers, L. Mullen, B. Concannon, J. Davis, J. Prentice, and V. Contarino. "The a,b,c's of oceanographic lidar predictions: a significant step towards closing the loop between theory and experiment," *Journal of Modern Optics,* vol. 49, no. 3/4, pp. 439-451 (2002).

[14] C.-L. Chen. *Elements of Optoelectronics & Fiber Optics*. Chicago: Irwin (1996).